



Strong Modulation of Spin Currents in Bilayer Graphene by Static and Fluctuating Proximity Exchange Fields

Simranjeet Singh,¹ Jyoti Katoch,¹ Tiancong Zhu,¹ Keng-Yuan Meng,¹ Tianyu Liu,^{2*}
Jack T. Brangham,¹ Fengyuan Yang,¹ Michael E. Flatté,² and Roland K. Kawakami¹

¹*Department of Physics, The Ohio State University, Columbus, Ohio 43210, USA*

²*Optical Science and Technology Center and Department of Physics and Astronomy,
University of Iowa, Iowa City, Iowa 52242, USA*

(Received 18 October 2016; revised manuscript received 19 January 2017; published 2 May 2017)

Two-dimensional materials provide a unique platform to explore the full potential of magnetic proximity-driven phenomena, which can be further used for applications in next-generation spintronic devices. Of particular interest is to understand and control spin currents in graphene by the magnetic exchange field of a nearby ferromagnetic material in graphene–ferromagnetic-insulator (FMI) heterostructures. Here, we present the experimental study showing the strong modulation of spin currents in graphene layers by controlling the direction of the exchange field due to FMI magnetization. Owing to clean interfaces, a strong magnetic exchange coupling leads to the experimental observation of complete spin modulation at low externally applied magnetic fields in short graphene channels. Additionally, we discover that the graphene spin current can be fully dephased by randomly fluctuating exchange fields. This is manifested as an unusually strong temperature dependence of the nonlocal spin signals in graphene, which is due to spin relaxation by thermally induced transverse fluctuations of the FMI magnetization.

DOI: [10.1103/PhysRevLett.118.187201](https://doi.org/10.1103/PhysRevLett.118.187201)

The use of the spin degree of freedom of electrons is poised to revolutionize next-generation devices for logic [1] and memory [2] applications. The manipulation of a spin current, using either a small electric or magnetic field, is the essential operation of such a device and is required to exploit the full versatility of spin-related phenomena. Spins in graphene are of particular interest because of the fact that spins can propagate over large distances due to small spin-orbit (SO) coupling and negligible hyperfine interaction [3,4]. However, the absence of a strong SO field in graphene also means that spins in graphene cannot be manipulated by an external applied electric field [5]. In general, spins in graphene are manipulated by an out-of-plane magnetic field [6,7], known as Hanle spin precession, requiring large fields which are not viable for applications. An alternative route for efficient spin manipulation is to use the magnetic proximity effect of an adjacent ferromagnetic insulator (FMI). Two-dimensional (2D) materials, like graphene, provide a unique platform to explore the proximity-induced phenomena, as these effects are expected to be the strongest in 2D materials. There has been a great deal of interest to study the proximity-effect-induced changes in the electrical [8], optical [9,10], and spin [11] related properties of low-dimensional materials. This research direction is further propelled by recent progress in the experimental techniques to assemble clean van der Waals heterostructures of 2D materials or mechanically transfer 2D samples onto arbitrary materials [12,13]. Recently, magnetic proximity effects in graphene-FMI heterostructures has been explored by charge transport measurements:

(i) the demonstration of ferromagnetism in graphene coupled to yttrium iron garnet (YIG) [14] and (ii) large magnetic exchange fields experienced by charge carriers in graphene/EuS heterostructures [15]. Undoubtedly, these studies have established the presence of strong magnetic coupling across the interfaces of graphene and FMI materials, opening the doors for studying spin currents in graphene under the influence of a magnetic proximity effect [16]. In particular, bilayer graphene is a system of choice for exploring these experiments due to the long spin diffusion lengths and spin lifetimes [17–19], electric-field-induced band gap engineering [20], and the feasibility of electric-field-driven spin rotation [21].

In this Letter, we report the complete modulation of spin currents in bilayer graphene using the static and/or fluctuating components of the magnetic exchange field of an adjacent ferromagnet in a graphene-FMI heterostructure. For the control of spin currents by a static exchange field, we employ a bilayer graphene lateral spin valve device on a YIG substrate and modulate the spin current in graphene by changing the direction of the YIG magnetization. A strong interfacial magnetic exchange coupling leads to the experimental observation of complete spin modulation in short graphene channels and at low magnetic fields. In addition, we discover that the spin current can be fully modulated by randomly fluctuating exchange fields. This is manifested as an unusually strong temperature dependence of the nonlocal spin signals, compared to the weak temperature dependence typically observed for graphene on nonmagnetic substrates [3,22]. We attribute this to spin relaxation

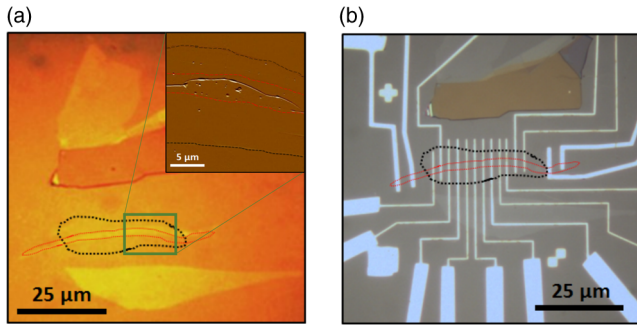


FIG. 1. (a) Optical image of an h-BN/graphene stack on a YIG substrate. Inset: Atomic force microscopy image of the h-BN/graphene/YIG heterostructure surface after vacuum annealing. (b) Optical image of the completed spin valve device. The red and black dotted lines in (a) and (b) outline the graphene and h-BN tunnel barrier boundaries, respectively.

by thermally induced transverse fluctuations of the YIG magnetization. These studies establish a lower bound on the magnetic exchange field to be ~ 1 T.

We choose YIG for the ferromagnet, because it is an insulator, has a high Curie temperature, is chemically stable under ambient conditions, and is magnetically soft [23,24]. To prepare clean heterostructures of graphene-YIG, we employ a dry transfer technique [13,25] as discussed in Supplemental Material [26]. The optical image of the hexagonal boron nitride (h-BN)/graphene stack on YIG is shown in Fig. 1(a), where thin h-BN is highlighted by black dotted lines. The AFM topography of the h-BN/graphene/YIG surface is depicted in Fig. 1(a) with the clean interface. In this structure, the h-BN serves as the tunnel barrier for spin injection into graphene [25]. Figure 1(b) shows the optical image of the device where the graphene and h-BN flakes are outlined with red and black dotted lines, respectively.

First, we establish the spin transport in a bilayer graphene channel ($2.1 \mu\text{m}$ long and $2.2 \mu\text{m}$ wide) on YIG by measuring the nonlocal magnetoresistance (MR). While sweeping an in-plane magnetic field, along y -axis in Fig. 2(a), we record the nonlocal voltage signal (V_{NL}). Figure 2(b) shows R_{NL} ($R_{\text{NL}} = V_{\text{NL}}/I$) as a function of the in-plane magnetic field. The schematic of the experiment, to demonstrate control over spin currents in graphene by a magnetic proximity effect, is shown in Fig. 2(a). To modulate the spin signal in graphene, we align the magnetization of electrodes $E2$ and $E3$ in either a parallel (P) or antiparallel (AP) configuration and apply a fixed magnitude of magnetic field, $B_{\text{ROT}} = 15$ mT, in the plane of the graphene. Note that this magnetic field is smaller than what is required to change or switch the electrode but large enough to saturate the YIG magnetization [19]. This magnetic field is rotated in the plane of the graphene by angle θ . Figure 2(c) shows R_{NL} as a function of θ for the P configuration (blue circles) and AP configuration (red circles). We observe a clear modulation of the nonlocal signals for both P and AP configurations. To calculate the net change of the observed signal, we show in Fig. 2(d) the differential R_{NL} between the P and AP

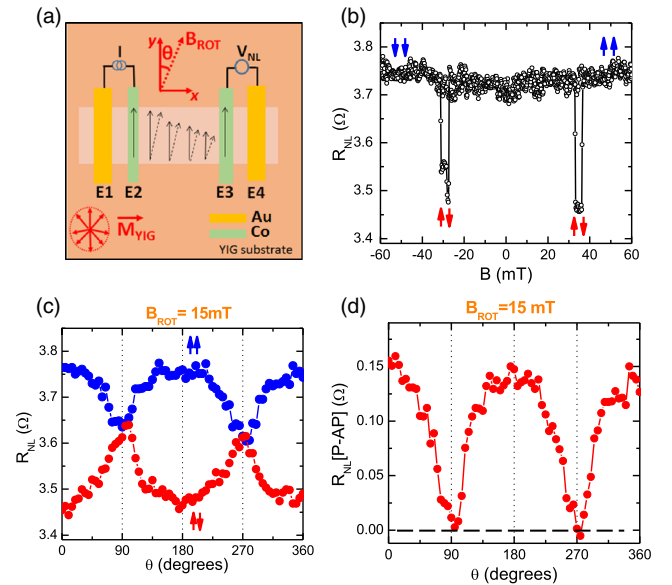


FIG. 2. Spin signal modulation in graphene coupled to a YIG substrate at 15 K. (a) Schematic of the experiment used to demonstrate spin current modulation in graphene. A magnetic field (B_{ROT}) applied at different θ defines the YIG magnetization (M_{YIG}) relative to the magnetization of Co injector/detector electrodes (or injected spin polarization in graphene). (b) The measured non-local MR signal in a graphene spin valve on YIG. The blue and red arrows represent the relative magnetization direction of injector ($E2$) and detector ($E3$) electrodes. (c) Non-local MR signal measured as function of B_{ROT} magnetic field direction (θ). A fixed $B_{\text{ROT}} = 15$ mT is applied in the YIG plane. The blue and red filled circles show the measured data for parallel and anti-parallel configuration of the injector/detector electrodes, respectively. (d) Differential non-local MR between the parallel and anti-parallel data from (c) as a function of θ , showing that for $\theta = 90^\circ$, the signal goes to zero which indicates a complete spin dephasing.

configurations. The change in spin signal due to the controlled change of the YIG magnetization direction can be defined as $\delta R = R(\theta = 0^\circ) - R(\theta)/R(\theta = 0^\circ)$, and one would expect to have maximum dephasing of the spins for B_{ROT} applied at $\theta = 90^\circ$. This is indeed what we observe as the nonlocal MR signal goes to zero for a magnetic field applied at $\theta = 90^\circ$ and corresponds to 100% modulation. In other words, when the YIG magnetization is transverse to the injected spin polarization, there is a complete dephasing of the injected spins in the graphene channel.

By performing control experiments, we show that this modulation is primarily due to the proximity exchange field B_{ex} ($\sim M_{\text{YIG}}$), originating from quantum mechanical interactions of the carriers in graphene with the YIG magnetization, as opposed to a direct effect of the external field B_{ROT} . One possible effect of B_{ROT} is to tilt the Co magnetizations asymmetrically to reduce R_{NL} . This effect is ruled out through anisotropic magnetoresistance measurements of the Co electrodes [34,35], as discussed in Supplemental Material [26]. The other possible effect of

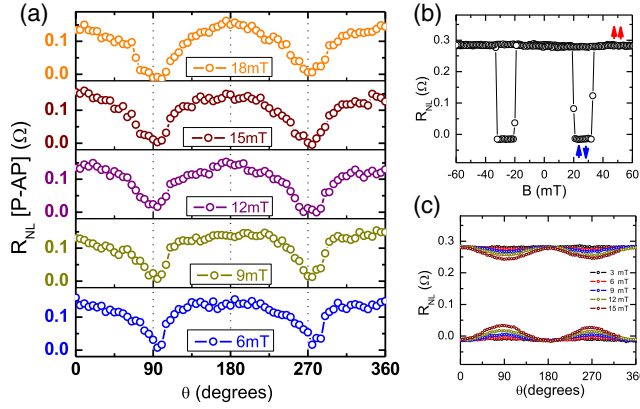


FIG. 3. Dependence of spin signal modulation on the magnitude of B_{ROT} . (a) Spin signal modulation, $R_{NL}[P - AP]$, for B_{ROT} ranging from 6 to 18 mT for a graphene device on YIG shows that the spin signal modulation is independent of the magnitude of B_{ROT} . (b) Non-local MR signal for a bilayer graphene on a non-magnetic SiO_2/Si substrate with the relative magnetization orientations of the electrodes denoted by the red and blue arrows. (c) Spin signal modulation as function of θ for a graphene device on SiO_2/Si at different applied B_{ROT} fields between 6 and 15 mT for both parallel and anti-parallel configurations.

B_{ROT} is the direct interaction with the carriers in graphene to dephase the spin polarization via Hanle spin precession. Indeed, with the presence of a proximity exchange field, the Hanle spin precession should be governed by the total magnetic field $B_{total} = B_{ex} + B_{ROT}$. The relative importance of B_{ex} and B_{ROT} can be determined by performing angular scans (θ) for different magnitudes of B_{ROT} . If B_{ex} dominates, there should be very little dependence on $|B_{ROT}|$, because M_{YIG} is fully saturated for fields higher than a few mT [26] and B_{ex} is proportional to M_{YIG} . If the direct interaction of B_{ROT} dominates, then the modulation should become stronger with increasing $|B_{ROT}|$. Figure 3(a) shows the angular scan of R_{NL} vs θ for different values of $|B_{ROT}|$ from 6 to 18 mT. The most striking feature is the similarity of all the curves, which show full modulation even for the lower applied magnetic fields. This indicates that the modulation is dominated by the proximity exchange field. We further test this conclusion by performing the same measurement of a control sample consisting of a bilayer graphene spin valve on a $\text{SiO}_2/\text{Si}(001)$ substrate. The measured nonlocal MR signal is shown in Fig. 3(b). The nonlocal signal as a function of θ for different values of $|B_{ROT}|$, measured for both parallel and antiparallel configurations of injector or detector electrodes, is shown in Fig. 3(c). Clearly, we observe a highest modulation of only a few percent ($\sim 10\%$) in contrast to the 100% modulation when graphene is placed on a YIG substrate. Furthermore, we have also carried out a spin modulation experiment on another control sample, wherein graphene is separated from YIG by a thin h-BN (gra/h-BN/YIG) and we do not observe nonlocal spin signal modulation more than a few percent (see Supplemental Material [26]). Thus, for graphene on a

nonmagnetic substrate, the modulation by B_{ROT} is much weaker and has a strong dependence on the magnitude of the field consistent with the Hanle effect.

Next, we study the temperature dependence of a spin signal in the graphene channel coupled to YIG, which reveals a new mechanism for spin relaxation due to fluctuating proximity exchange fields. The magnitude of the measured MR signal (ΔR_{NL}) is defined as the difference of R_{NL} between the parallel and antiparallel configurations [Fig. 2(b)], and the measured value is approximately 0.22 Ω at 15 K. Then, we measure ΔR_{NL} at different temperatures, and the observed data are shown in Fig. 4(a). The spin signal in graphene on a nonmagnetic substrate normally has a weak temperature dependence and decreases approximately by a factor of 2 (or so) going from 10 K to room temperature [22,36,37]. However, as clearly seen from Fig. 4(a), we observe that the spin signal rapidly decays as the temperature increases and completely disappears at ~ 230 K. Because the nonlocal spin signal is known to be dependent on the graphene resistivity ρ and the interfacial contact resistances of the electrodes [3], we first check whether these can account for the observed temperature dependence of ΔR_{NL} . The temperature dependence of the graphene sheet resistance (or resistivity) on YIG is shown in Fig. 4(b) and is similar to what has been widely reported for graphene on other nonmagnetic substrates [12,22,38,39]. We also point out that the interfacial contact resistances of both injector and detector electrodes stay constant over the measured temperature range as shown in Fig. 4(c). This rules out that the strong temperature-dependent decay of the spin signal is merely due to changes in ρ or the contact resistances. Additionally, we have measured the temperature dependence of MR signals in the gra/h-BN/YIG control sample (Supplemental Material) and did not observe a strong temperature dependence [26]. In the following, we argue that the observed temperature dependence of the MR spin signal in graphene-YIG can be explained by the electron spin dephasing in graphene due to the random transverse magnetization fluctuations of the YIG film. To qualitatively understand this unusual temperature dependence of the spin signal, we consider the interaction between conduction electrons in graphene and the magnetization of YIG. The terms in the Hamiltonian associated with the conduction electron spins are given by

$$\begin{aligned} H_e &= A_{ex} g_e \mu_B \vec{S}_e \cdot \langle \vec{M} \rangle + g_e \mu_B \vec{S}_e \cdot \vec{B}_{app} \\ &= g_e \mu_B \vec{S}_e \cdot (\langle \vec{B}_{ex} \rangle + \vec{B}_{app}) \\ &= g_e \mu_B \vec{S}_e \cdot \langle \vec{B}_{eff} \rangle, \end{aligned} \quad (1)$$

where A_{ex} is the proximity-induced exchange coupling strength between YIG and graphene, \vec{M} is the YIG magnetization, and $\langle \vec{B}_{ex} \rangle = A_{ex} \langle \vec{M} \rangle$ is the effective exchange field. The averaging $\langle \dots \rangle$ is over the ensemble of magnetic moments in YIG that are in proximity with graphene. At a finite temperature, \vec{M} in YIG fluctuates, which in turn causes

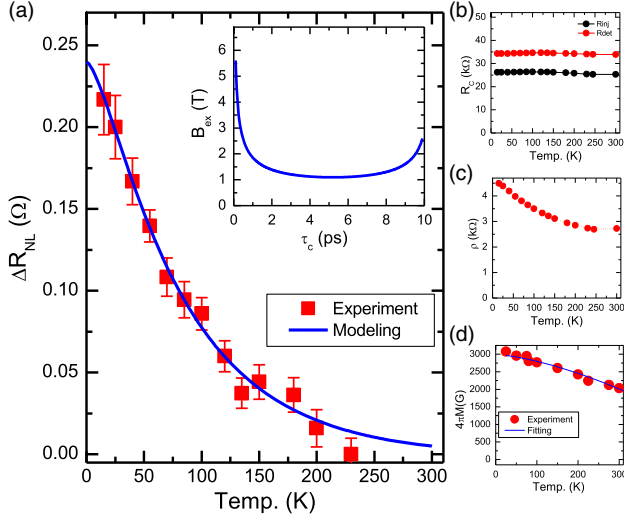


FIG. 4. (a) Temperature dependence of non-local MR signal in a graphene spin valve on YIG, where the red filled squares are experimental data and the blue solid line is the fitting by a model based on spin dephasing due to the temperature dependent transverse magnetization fluctuations of YIG. Inset: Extracted exchange field as function of correlation time of fluctuating YIG magnetization. (b) Temperature dependence of graphene sheet resistance. (c) Temperature dependence of interfacial contact resistances of the injector (black) and detector (red) electrodes. (d) Temperature dependence of saturation magnetization (red filled circles) of the YIG film extracted from magnetization measurements. The solid blue line is a fitting of the temperature dependent magnetization data by Eq. (4).

the proximity exchange field in graphene to fluctuate as well. For an electron traveling through graphene, the time and spatial variation of the magnetization in YIG results in a varying effective magnetic field acting on the electron spin. This varying effective magnetic field can be modeled as a time-dependent, randomly fluctuating magnetic field $\vec{B}_{\text{ex}}(t) = \langle \vec{B}_{\text{ex}} \rangle + \Delta \vec{B}_{\text{ex}}$. Previous theoretical work had predicted that the randomly fluctuating magnetic field can cause extra spin relaxation [40,41] and has been used to explain spin transport phenomena in graphene decorated with paramagnetic hydrogen adatoms [42]. Furthermore, the fluctuation strength of YIG magnetization is expected to be temperature dependent. As a result, the spin relaxation rate caused by the magnetization fluctuation should be temperature dependent as well. In the following, we use the above model to understand the observed temperature dependence data. For nonlocal geometry [Fig. 2(a)], the injected spin polarization, the applied magnetic field, and the effective exchange field lie along the same axis (y axis in our case). The spin relaxation rate induced by the random fluctuating field is given by the longitudinal spin relaxation term:

$$\frac{1}{\tau_1^{\text{ex}}} = \frac{(\Delta B_{\text{tr}})^2}{\tau_c} \frac{1}{(B_{\text{app},y} + \bar{B}_{\text{ex},y})^2 + (\gamma_e \tau_c)^{-2}} \approx \frac{(\Delta B_{\text{tr}})^2}{\tau_c} \frac{1}{(\bar{B}_{\text{ex},y})^2 + (\gamma_e \tau_c)^{-2}}, \quad (2)$$

where $(\Delta B_{\text{tr}})^2 = (\Delta B_{\text{ex},x})^2 + (\Delta B_{\text{ex},z})^2$ is the fluctuation of the exchange field in the transverse direction, $B_{\text{app},y}$ is ignored as $\bar{B}_{\text{ex},y} \gg B_{\text{app},y}$, γ_e is the gyromagnetic ratio of the electron, and τ_c is the correlation time of the exchange field fluctuation defined as $\Delta \langle \vec{B}_{\text{ex}}(t) \cdot \vec{B}_{\text{ex}}(t-t') \rangle_t \propto \exp(-t/\tau_c)$. The exchange field fluctuation in graphene should be strongly associated with the magnetization fluctuation of YIG. At a finite temperature, thermally driven magnetization fluctuations suppress the equilibrium magnetization from the saturated 0 K value. Assuming that transverse magnetization fluctuations in YIG are responsible for the reduction of M with increasing temperature, we can rewrite Eq. (2) as

$$\frac{1}{\tau_1^{\text{ex}}} = \frac{A_{\text{ex}}^2 \{ (M_0)^2 - [\bar{M}_y(T)]^2 \}}{\tau_c \{ [A_{\text{ex}} \bar{M}_y(T)]^2 + [\gamma_e \tau_c(T)]^{-2} \}}, \quad (3)$$

where M_0 is the saturation magnetization of YIG at 0 K, $\bar{M}_y(T)$ is the temperature-dependent equilibrium magnetization in the y direction, and $\tau_c(T)$ is the temperature-dependent correlation time. We extract the temperature dependence of \bar{M}_y from the measured temperature dependence of the saturation magnetization of YIG up to 300 K [Fig. 4(d)]. A previous study of bulk YIG shows that the reduction of saturation magnetization follows $\sim T^{3/2}$ in the low temperature regime (< 25 K), while it follows a $\sim T^3$ in the higher temperature regime (25–250 K) [43]. We fit the measured data with both terms and find that the contribution of the T^3 term is minimal. To simplify the spin transport equation later, we assume that

$$\frac{\bar{M}_y}{M_0} = 1 - aT^{3/2} \quad (4)$$

and get $a = 6.314 \times 10^{-5} \text{ K}^{-3/2}$ from fitting with the experimental YIG magnetization.

To obtain the temperature dependence of the correlation time, we have adapted a macroscopic picture of local magnetization fluctuation which has been developed through the fluctuation-dissipation theorem and had successfully explained the spin Seebeck effect in a Pt/YIG structure [44–46]. As explained in detail in Supplemental Material [26], the relationship between the correlation time and YIG magnetization is

$$\frac{1}{\tau_c(T)} = \frac{\alpha}{\sqrt{1 + \alpha^2}} \omega_0 = \frac{\alpha \gamma H_0}{\sqrt{1 + \alpha^2}} = \eta M_{\text{YIG}}(T). \quad (5)$$

To simplify the expression of τ_1^{ex} , we put Eqs. (4) and (5) into Eq. (3):

$$\frac{1}{\tau_1^{\text{ex}}} = \frac{A_{\text{ex}}^2 \{ (M_0)^2 - [\bar{M}_y(T)]^2 \}}{\tau_c \{ [A_{\text{ex}} \bar{M}_y(T)]^2 + [\gamma_e \tau_c(T)]^{-2} \}} = \frac{1 - (\bar{M}_y/M_0)^2}{\bar{M}_y/M_0} \frac{\eta (\gamma_e A_{\text{ex}})}{(\gamma_e A_{\text{ex}})^2 + \eta^2} \gamma_e A_{\text{ex}} M_0. \quad (6)$$

We define $\xi(T) = [1 - (\bar{M}_y/M_0)^2]/\bar{M}_y/M_0$, which is the only temperature-dependent term, and rewrite the whole equation as

$$\frac{1}{\tau_1^{\text{ex}}} = \xi(T) \frac{\eta(\gamma_e A_{\text{ex}})}{(\gamma_e A_{\text{ex}})^2 + \eta^2} \gamma_e A_{\text{ex}} M_0. \quad (7)$$

The nonlocal spin signal measured in the graphene lateral spin valve device can be written as [32,37]

$$R_{\text{NL}} = p_1 p_2 R_N e^{-L/\lambda}, \quad (8)$$

where p_1 and p_2 are the spin polarizations at the Co/h-BN/graphene injector and detector junctions, respectively, $\lambda = \sqrt{D\tau_{\text{total}}}$ is the spin diffusion length, R_N is the spin resistance of the graphene channel, D is the diffusion constant, and τ_{total} is the spin lifetime of electron spins in graphene. Apart from the spin relaxation mechanism in graphene on a nonmagnetic substrate, in our case we have additional spin relaxation $1/\tau_1^{\text{ex}}$ caused by the YIG magnetization fluctuations [Eq. (3)]. Thus, Eq. (8) becomes

$$R_{\text{NL}} = p_1 p_2 R_N e^{-L/(D\tau_1^{\text{ex}} + 1/\lambda_{\text{int}}^2)^{-1/2}}, \quad (9)$$

where λ_{int} is the spin diffusion length of graphene for the case of a nonmagnetic substrate. Using Eq. (9), we obtain

$$R_{\text{NL}} = \mathcal{R} e^{-L(\xi(T)/\beta + 1/\lambda_{\text{int}}^2)^{-1/2}}, \quad (10)$$

where $1/\beta = \gamma_e/D\{\eta(\gamma_e A_{\text{ex}})/[(\gamma_e A_{\text{ex}})^2 + \eta^2]\}A_{\text{ex}}M_0$. Using $L = 2.1 \mu\text{m}$ (channel length), we fit the observed temperature dependence of the nonlocal MR signal. The model fits very well with the experimental data as shown in Fig. 4(a), from which we can extract $\mathcal{R} = 0.7015 \Omega$, $\lambda_{\text{int}} = 1.9561 \mu\text{m}$, and $\beta = 1.5578 \times 10^{-13} \text{ m}^2$.

To calculate the exchange field in graphene at 0 K, we focus on the β coefficient from the fitting using

$$B_{\text{ex}}(0) = A_{\text{ex}}M_0 = \sqrt{\frac{D}{\eta\beta M_0 - D}} \frac{\eta M_0}{\gamma_e} = \frac{1}{\gamma_e} \sqrt{\frac{1}{(\beta/D)\tau_c - \tau_c^2}}, \quad (11)$$

where τ_c is the correlation time at 0 K. Assuming a typical $D = 0.015 \text{ m}^2/\text{s}$ for graphene [3,25,37], we plot $B_{\text{ex}}(0)$ as a function of different τ_c as shown in the inset of Fig. 4(a). Our model gives a lower bound of 1 T of the exchange field. We also measure the temperature dependence of the spin signal modulation and observe a clear 100% signal modulation up to ~ 150 K, where we have clear MR signals, confirming the existence of this magnetic proximity-induced phenomena at higher temperatures [26].

In conclusion, we have experimentally demonstrated the full modulation of spins in graphene by employing the proximity exchange fields present at the interface of a graphene-FMI heterostructure. The observed strong temperature dependence of nonlocal MR signals in

graphene spin valves for the first time experimentally establishes the additional spin dephasing mechanism due to the magnetic fluctuations in graphene-ferromagnet systems. We have used this novel observation to extract a lower bound of the interfacial magnetic exchange field. The work presented here will further help understand (and also exploit) the interfacial effects due to the interaction of spins and magnetization in ferromagnet or nonmagnetic bilayer systems in general.

S. S., J. K., T. Z., and R. K. K. acknowledge support from Office of Naval Research (No. N00014-14-1-0350), National Science Foundation (NSF) (No. DMR-1310661), Army Research Office (W911NF-11-1-0182), and C-SPIN, one of the six SRC STARnet Centers, sponsored by Microelectronics Advanced Research Corporation (MARCO) and Defense Advanced Research Projects Agency (DARPA). K. Y. M. acknowledges support from NSF (No. DMR-1507274). T. L. and M. F. acknowledge support from C-SPIN, one of the six SRC STARnet Centers, sponsored by MARCO and DARPA. J. T. B. and F. Y. Y. acknowledge support from U. S. Department of Energy, Office of Science, Basic Energy Sciences, under Award No. DE-SC0001304. This work received partial support from the Center for Emergent Materials: an NSF MRSEC under Award No. DMR-1420451. We also thank Walid Amamou, Jinsong Xu, and Igor Pinchuk for technical assistance.

*Present address: Department of Physics, Tianjin University, Tianjin 300350, China.

- [1] B. Behin-Aein, D. Datta, S. Salahuddin, and S. Datta, *Nat. Nanotechnol.* **5**, 266 (2010).
- [2] L. Liu, C. F. Pai, Y. Li, H. W. Tseng, D. C. Ralph, and R. A. Buhrman, *Science* **336**, 555 (2012).
- [3] W. Han, R. K. Kawakami, M. Gmitra, and J. Fabian, *Nat. Nanotechnol.* **9**, 794 (2014).
- [4] M. Wojtaszek, I. J. Vera-Marun, E. Whiteway, M. Hilke, and B. J. van Wees, *Phys. Rev. B* **89**, 035417 (2014).
- [5] H. C. Koo, J. H. Kwon, J. Eom, J. Chang, S. H. Han, and M. Johnson, *Science* **325**, 1515 (2009).
- [6] N. Tombros, C. Jozsa, M. Popinciuc, H. T. Jonkman, and B. J. van Wees, *Nature (London)* **448**, 571 (2007).
- [7] W. Han, K. Pi, W. Bao, K. M. McCreary, Y. Li, W. H. Wang, C. N. Lau, and R. K. Kawakami, *Appl. Phys. Lett.* **94**, 222109 (2009).
- [8] C. R. Dean, L. Wang, P. Maher, C. Forsythe, F. Ghahari, Y. Gao, J. Katoch, M. Ishigami, P. Moon, M. Koshino, T. Taniguchi, K. Watanabe, K. L. Shepard, J. Hone, and P. Kim, *Nature (London)* **497**, 598 (2013).
- [9] S. Wu, L. Wang, Y. Lai, W.-Y. Shan, G. Aivazian, X. Zhang, T. Taniguchi, K. Watanabe, D. Xiao, C. Dean, J. Hone, Z. Li, and X. Xu, *Sci. Adv.* **2**, e1600002 (2016).
- [10] P. Rivera, K. L. Seyler, H. Yu, J. R. Schaibley, J. Yan, D. G. Mandrus, W. Yao, and X. Xu, *Science* **351**, 688 (2016).
- [11] M. H. D. Guimarães, P. J. Zomer, J. Ingla-Aynés, J. C. Brant, N. Tombros, and B. J. van Wees, *Phys. Rev. Lett.* **113**, 086602 (2014).

- [12] C. R. Dean, A. F. Young, I. Meric, C. Lee, L. Wang, S. Sorgenfrei, K. Watanabe, T. Taniguchi, P. Kim, K. L. Shepard, and J. Hone, *Nat. Nanotechnol.* **5**, 722 (2010).
- [13] L. Wang, I. Meric, P. Y. Huang, Q. Gao, Y. Gao, H. Tran, T. Taniguchi, K. Watanabe, L. M. Campos, D. A. Muller, J. Guo, P. Kim, J. Hone, K. L. Shepard, and C. R. Dean, *Science* **342**, 614 (2013).
- [14] Z. Wang, C. Tang, R. Sachs, Y. Barlas, and J. Shi, *Phys. Rev. Lett.* **114**, 016603 (2015).
- [15] P. Wei, S. Lee, F. Lemaitre, L. Pinel, D. Cutaia, W. Cha, F. Katmis, Y. Zhu, D. Heiman, J. Hone, J. S. Moodera, and C. T. Chen, *Nat. Mater.* **15**, 711 (2016).
- [16] J. C. Leutenantsmeyer, A. A. Kaverzin, M. Wojtaszek, and B. J. van Wees, *2D Mater.* **4**, 014001 (2017).
- [17] T. Y. Yang, J. Balakrishnan, F. Volmer, A. Avsar, M. Jaiswal, J. Samm, S. R. Ali, A. Pachoud, M. Zeng, M. Popinciuc, G. Güntherodt, B. Beschoten, and B. Özyilmaz, *Phys. Rev. Lett.* **107**, 047206 (2011).
- [18] W. Han and R. K. Kawakami, *Phys. Rev. Lett.* **107**, 047207 (2011).
- [19] A. Avsar, I. J. Vera-Marun, J. Y. Tan, G. K. W. Koon, K. Watanabe, T. Taniguchi, S. Adam, and B. Özyilmaz, *NPG Asia Mater.* **8**, e274 (2016).
- [20] Y. Zhang, T. T. Tang, C. Girit, Z. Hao, M. C. Martin, A. Zettl, M. F. Crommie, Y. R. Shen, and F. Wang, *Nature (London)* **459**, 820 (2009).
- [21] P. Michetti, P. Recher, and G. Iannaccone, *Nano Lett.* **10**, 4463 (2010).
- [22] M. V. Kamalakar, A. Dankert, J. Bergsten, T. Ive, and S. P. Dash, *Sci. Rep.* **4**, 6146 (2014).
- [23] H. L. Wang, C. H. Du, Y. Pu, R. Adur, P. C. Hammel, and F. Y. Yang, *Phys. Rev. B* **88**, 100406 (2013).
- [24] H. L. Wang, C. H. Du, Y. Pu, R. Adur, P. C. Hammel, and F. Y. Yang, *Phys. Rev. Lett.* **112**, 197201 (2014).
- [25] S. Singh, J. Katoch, J. Xu, C. Tan, T. Zhu, W. Amamou, J. Hone, and R. Kawakami, *Appl. Phys. Lett.* **109**, 122411 (2016).
- [26] See Supplemental Material at <http://link.aps.org/supplemental/10.1103/PhysRevLett.118.187201>, which includes Refs. [27–33], for details about heterostructure preparation, control experiments, and details of the modeling.
- [27] L. M. Malard, J. Nilsson, D. C. Elias, J. C. Brant, F. Plentz, E. S. Alves, A. H. Castro Neto, and M. A. Pimenta, *Phys. Rev. B* **76**, 201401 (2007).
- [28] A. C. Ferrari, J. C. Meyer, V. Scardaci, C. Casiraghi, M. Lazzeri, F. Mauri, S. Piscanec, D. Jiang, K. S. Novoselov, S. Roth, and A. K. Geim, *Phys. Rev. Lett.* **97**, 187401 (2006).
- [29] W. F. Brown, *Phys. Rev.* **130**, 1677 (1963).
- [30] R. Kubo, M. Toda, and N. Hashitsume, *Statistical Physics: II. Nonequilibrium Statistical Mechanics* (Springer, Berlin, 1991).
- [31] L. D. Landau and E. M. Lifshitz, *Statistical Physics: Part I* (Pergamon, Oxford, 1980).
- [32] W. Han, K. Pi, K. M. McCreary, Y. Li, J. J. I. Wong, A. G. Swartz, and R. K. Kawakami, *Phys. Rev. Lett.* **105**, 167202 (2010).
- [33] B. Raes, J. E. Scheerder, M. V. Costache, F. Bonell, J. F. Sierra, J. Cuppens, J. Van de Vondel, and S. O. Valenzuela, *Nat. Commun.* **7**, 11444 (2016).
- [34] E. Villamor, M. Isasa, S. Vélez, A. Bedoya-Pinto, P. Vavassori, L. E. Hueso, F. S. Bergeret, and F. Casanova, *Phys. Rev. B* **91**, 020403 (2015).
- [35] F. K. Dejene, N. Vlietstra, D. Luc, X. Waintal, J. Ben Youssef, and B. J. van Wees, *Phys. Rev. B* **91**, 100404 (2015).
- [36] Y. Takehiro, I. Yoshihisa, M. Satoru, M. Sei, O. Masahiro, W. Kenji, T. Takashi, M. Rai, and M. Tomoki, *Appl. Phys. Express* **6**, 073001 (2013).
- [37] W. Han, K. M. McCreary, K. Pi, W. H. Wang, Y. Li, H. Wen, J. R. Chen, and R. K. Kawakami, *J. Magn. Magn. Mater.* **324**, 369 (2012).
- [38] Y. Liu, W. Li, M. Qi, X. Li, Y. Zhou, and Z. Ren, *Physica (Amsterdam)* **69E**, 115 (2015).
- [39] J. B. Oostinga, H. B. Heersche, X. Liu, A. F. Morpurgo, and L. M. K. Vandersypen, *Nat. Mater.* **7**, 151 (2007).
- [40] E. L. Hahn and A. Abragam, *Pulsed Magnetic Resonance-NMR, ESR, and Optics* (Clarendon, New York, 1992).
- [41] J. Fabian, A. Matos-Abiague, C. Ertler, P. Stano, and I. Zutic, *Acta Phys. Slovaca* **57**, 342 (2007).
- [42] K. M. McCreary, A. G. Swartz, W. Han, J. Fabian, and R. K. Kawakami, *Phys. Rev. Lett.* **109**, 186604 (2012).
- [43] V. Cherepanov, I. Kolokolov, and V. L'Vov, *Phys. Rep.* **229**, 81 (1993).
- [44] J. Xiao, G. E. W. Bauer, K. C. Uchida, E. Saitoh, and S. Maekawa, *Phys. Rev. B* **81**, 214418 (2010).
- [45] H. Adachi, J. I. Ohe, S. Takahashi, and S. Maekawa, *Phys. Rev. B* **83**, 094410 (2011).
- [46] H. Adachi, K. Uchida, E. Saitoh, and S. Maekawa, *Rep. Prog. Phys.* **76**, 036501 (2013).